Volumetric histograms-based analysis of apparent diffusion coefficients and standard uptake values for the assessment of pediatric sarcoma at staging: preliminary results of a PET/MRI study

Giovanna Orsatti[1] · Pietro Zucchetta[2] · Alessia Varotto[3] · Filippo Crimì[1] · Michael Weber[4] · Diego Cecchin[2] · Gianni Bisogno[5] · Alessandro Spimpolo[2] · Chiara Giraudo[1] · Roberto Stramare[1]

Abstract

Purpose To assess the relationship between apparent diffusion coefficients (ADC) and standard uptake values (SUV) of pediatric sarcomas at staging by using volumetric histograms analyses.

Methods Children with histologically proven sarcoma, referring to our tertiary center for a whole-body ^{18}F-FDG PET/MRI for staging and including diffusion weighted imaging in the MRI protocol were investigated. Firstly, turbo inversion recovery magnitude (TIRM) and PET images were resliced and resampled according to the ADC maps. Regions of interests were drawn along tumor margins on TIRM images and then copied on PET and ADC datasets. Pixel-based SUVs and ADCs were collected from the entire volume of each lesion. Mean, median, skewness, and kurtosis of SUVs and ADCs values were computed, and the Pearson correlation coefficient was then applied (for the entire population and for histological subgroups with more than five patients).

Results Thirteen patients met the inclusion criteria (six females; mean age 8.31 ± 6.03 years). Histology revealed nine rhabdomyosarcomas, three Ewing sarcomas, and one chondroblastic osteosarcoma. A significant negative correlation between ADCs' and SUVs' mean ($r_{mean} = -0.501$, $P < 0.001$), median ($r_{median} = -0.519$, $P < 0,001$), and skewness ($r_{skewness} = -0.550$, $P < 0.001$) emerged for the entire population and for rhabdomyosarcomas ($r_{mean} = -0.541$, $P = 0.001$, $r_{median} = -0.597$, $P < 0.001$, $r_{skewness} = -0.568$, $P < 0.001$), whereas a significant positive correlation was found for kurtosis ($r_{kurtosis} = 0.346$, $P < 0.001$, and $r_{kurtosis} = 0.348$, $P < 0.001$ for the entire population and for rhabdomyosarcomas, respectively).

Conclusion Our preliminary results demonstrate that, using volumetric histograms, simultaneously collected SUVs and ADCs are dependent biomarkers in pediatric FDG-avid sarcomas. Further studies, on a larger population, are necessary to confirm this evidence and assess its clinical implications.

Keywords Pediatric sarcoma · PET/MRI · ADC · SUV · Histograms

✉ Chiara Giraudo
  chiara.giraudo@unipd.it

1. Department of Medicine – DIMED, Institute of Radiology, Padova University, Via Giustiniani 2, 35100 Padua, Italy

2. Nuclear Medicine Unit, Department of Medicine – DIMED, University of Padova, Padua, Italy

3. Neuroradiology Unit, San Bortolo Hospital, Vicenza, Italy

4. Department of Biomedical Imaging and Image-Guided Therapy, Medical University of Vienna, Vienna, Austria

5. Hematology and Oncology Division, Department of Women's and Children's Health, University of Padova, Padua, Italy

Introduction

Sarcomas account for about 10% of all solid pediatric tumors and can be grouped in soft tissues and bone sarcomas. Soft tissue malignancies can be subdivided in two main groups: rhabdomyosarcoma and non-rhabdomyosarcoma. Rhabdomyosarcoma is the third most frequent extracranial pediatric solid tumor in children and adolescents, accounting for 5% of all pediatric cancers and for almost 50% of soft tissue sarcomas [1, 2]. Non-rhabdomyosarcomas represent around 7% of all pediatric malignancies and include different histotypes like non-osseous Ewing sarcoma, peripheral nerve sheath tumors, and synovial sarcoma [1, 3]. The most common malignant bone tumor in childhood is the osteosarcoma,

with a prevalence of 3–5%, followed by the osseous Ewing sarcoma [1].

Radiological imaging plays a significant role in the management of sarcomas. In particular, magnetic resonance imaging (MRI) is usually applied for assessing the primary tumor, while whole-body computed tomography (CT) is used for staging. Over the past few decades, the application of hybrid imaging has progressively increased since it allows the simultaneous collection of anatomical and metabolic information improving tumors' characterization. In particular, recently, there is growing interest on positron emission tomography (PET)/MRI, which carries several advantages in comparison with PET/CT [4, 5]. In fact, PET/MRI combines local and whole-body staging allowing also the use of peculiar sequences like diffusion weighted imaging (DWI) and MR spectroscopy [5–10].

Despite the growing body of evidence about DWI and PET/MRI, up to now, studies investigating the relationship between SUV and ADC using a volumetric approach in pediatric patients with sarcoma were still missing. Thus, aim of our project was to assess this relationship using simultaneously collected volumetric data extracted from pediatric sarcomas at staging, examined by PET/MRI.

Materials and methods

Patients

All patients' parents gave written informed consent before imaging. This retrospective study was approved by the Institutional Review Board.

Pediatric patients with histologically proven sarcoma (according to the World Health Organization Classification) referring to our tertiary center from January 2015 to July 2018 who underwent a whole-body ^{18}F-FDG PET/MRI examination for staging, including DWI of the primary lesion in the protocol, were included.

PET/MRI protocol

Patients fasted 4–6 h before the examination, keeping a proper hydration. Glucose hematic concentration was assessed, with a desirable value < 120 mg/dl (6.66 mmol/l). The dose of radiotracer was based on patient weight (3 MBq/kg). Patients were kept warm and at rest for 45–50 min after the ^{18}F-FDG injection. Sedation was performed in case of very young and less compliant patients.

Whole-body PET/MRI images were acquired with an integrated 3 T PET/MRI scanner (Biograph mMR, Siemens Healthcare, Germany). The PET/MR system consisted of a rigid 16-channel head/neck coil, a rigid 24-channel spine array coil, up to four flexible six-channel body matrix radiofrequency coils, an integrated PET scanner, installed between the gradient and radiofrequency coils, consisting of 8 rings of 56 detector blocks, 8×8 lutetium oxyorthosilicate crystals per block ($4 \times 4 \times 20$ mm), coupled to an array of 3×3 avalanche photodiodes. The axial range of each bed position was 25.8 cm with a 6.1-cm overlap between the adjacent bed positions.

Whole-body Dixon volumetric interpolated breath-hold examination (VIBE) MR images were used as attenuation correction maps. PET data were reconstructed by the 3D-ordered subset expectation maximization algorithm (3D-OSEM). A field of view (FOV) of 400 mm and a slice thickness of 3 mm have been applied. The MR protocol included the following whole-body sequences: axial T1-weighted (T1w) turbo spin echo, axial T2w half-Fourier-acquired single-shot turbo spin echo (HASTE), axial turbo inversion recovery magnitude (TIRM) (Table 1). A single-shot echo planar imaging sequence was used for DWI ($b = 50/1000$ s/mm^2). Fat-saturated VIBE images of the primary lesion were acquired before and after intravenous injection of gadolinium (gadoterate meglumine, 0.2 ml/kg). The total scan time was of ca. 50–60 min.

Table 1 Parameters of the magnetic resonance sequences included in the applied PET/MRI protocol

Sequence	TE (ms)	TR (ms)	TI (ms)	FOV read (mm)	FOV phase (%)	Base resolution	Slice thickness (mm)
T1w-TSE	8.6	508	–	400	95	320	5
HASTE	95	1600	–	380	95	320	5
TIRM	76	3160	220	400	95	320	4
VIBE	1.84	4.2	–	400	95	320	3
DWI	53	5000	–	380	95	100	5

TE = echo time; TR = repetition time; TI = inversion time; FOV = field of view; T1w = T1 weighted; TSE = turbo spin echo; HASTE = half-fourier acquisition single-shot turbo spin echo; TIRM = turbo inversion recovery magnitude; VIBE = volumetric interpolated breath-hold examination; DWI = diffusion weighted imaging

Images analyses

PET and MRI images were evaluated in consensus by one radiologist and one nuclear medicine physician respectively with five and fifteen years of experience in pediatric imaging. For each patient, only the primary tumor was considered for the analyses. All volumetric analyses were performed by an open-source software (OsiriX, v.8, https://www.osirix-viewer.com) applying multiple steps. Initially, to resize the datasets to the same dimensions, spacing, and origin, reslicing and resampling of PET, TIRM, and ADC images were performed. Then, a volumetric manual segmentation along the border of the primary tumor and throughout all slices were performed using the TIRM dataset. Each volumetric ROI was then applied on the PET and ADC datasets. Pixel-based SUV and ADC values of the entire volume were then collected (Fig. 1).

Statistical analysis

Descriptive statistics were applied for categorical data. Mean, median, skewness, and kurtosis of SUV and ADC values were computed. To evaluate the relationship between metabolic activity and cell-density, the Pearson correlation coefficient was applied for the entire population and, separately, for histological subgroups including more than five patients.

All statistical analyses were performed with SPSS (SPSS Statistics vr 24.0, IBM Corp, Armonk, NY).

Results

Thirteen patients met the inclusion criteria (seven males; mean age $\pm$ standard deviation (SD) 8.31 ± 6.03 years). Nine children were affected by rhabdomyosarcoma (i.e., five alveolar and four embryonal), three by osseous Ewing sarcoma and one by chondroblastic osteosarcoma (Fig. 2).

Nine patients had a localized disease, while four had distant metastases at diagnosis. Five primary lesions were in the leg, four in the hip/pelvis, two each in the head/neck and in the arm. The mean $\pm$ SD volume of the primary lesions at staging was of 114.73 ± 154.89 cm^3.

The distribution of mean, median, skewness, and kurtosis of the ADC and SUV values is represented in Fig. 3.

Regarding the volumetric analyses, considering the entire population, a moderate to good significant negative correlation occurred for ADCs' and SUVs' mean ($r_{mean} = -0.501$, $p < 0.001$), ADC and SUV median ($r_{median} = -0.519$, $p < 0.001$), and ADCs' and SUVs' skewness ($r_{skewness} = -0.550$, $p < 0.001$) (Fig. 4). A poor significant positive correlation between ADCs' and SUVs' kurtosis ($r_{kurtosis} = 0.346$, $p < 0.001$) was found (Fig. 4).
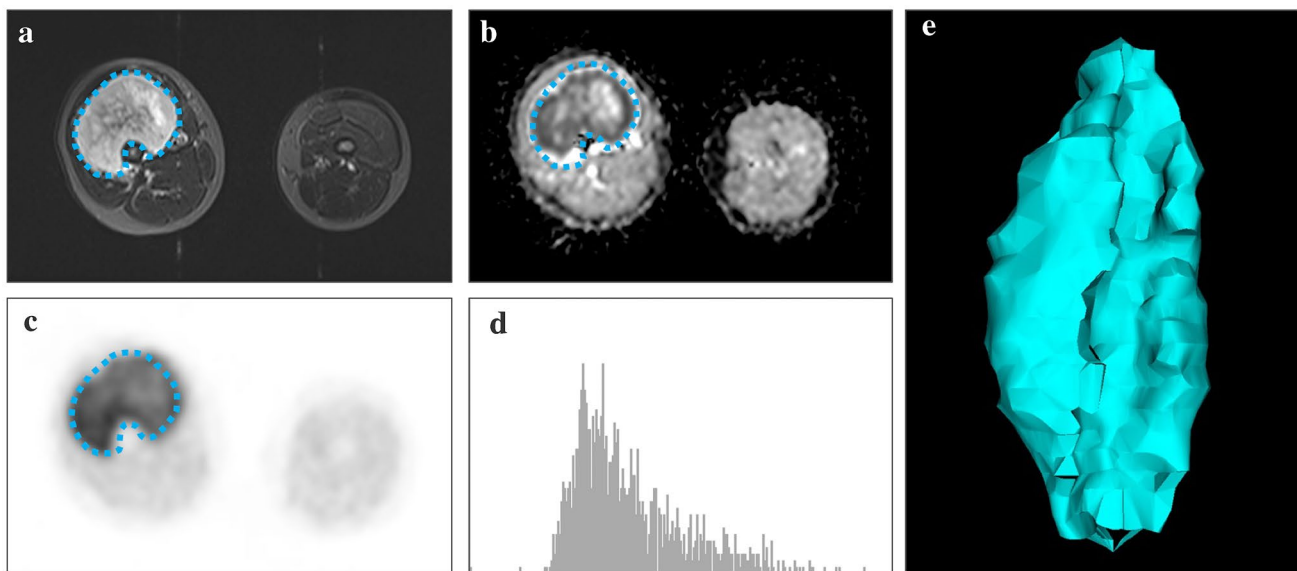

Fig. 1 Representation of the methodology applied to extract the pixels-based ADC and SUV values from the entire volumetric images, of each lesion, obtained by a fully integrated PET/MRI scanner. In particular, it is hereby represented a 10-year-old male with a rhabdomyosarcoma of the right quadriceps muscle characterized by high FDG uptake and restricted diffusion. A region of interest (ROI) was drawn on the turbo inversion recovery magnitude images on the axial plane (blue dotted line) covering the entire volume and then after reslicing and resampling, the same ROIs were copied on the ADC map (same blue dotted line in **b**) and PET dataset (same blue dotted line in **c**). All pixels were then extracted and analyzed. In **c** and **d** are represented, respectively, the histogram of the pixels obtained from the ADC map and the 3D volumetric reconstruction of the lesion of the same patient
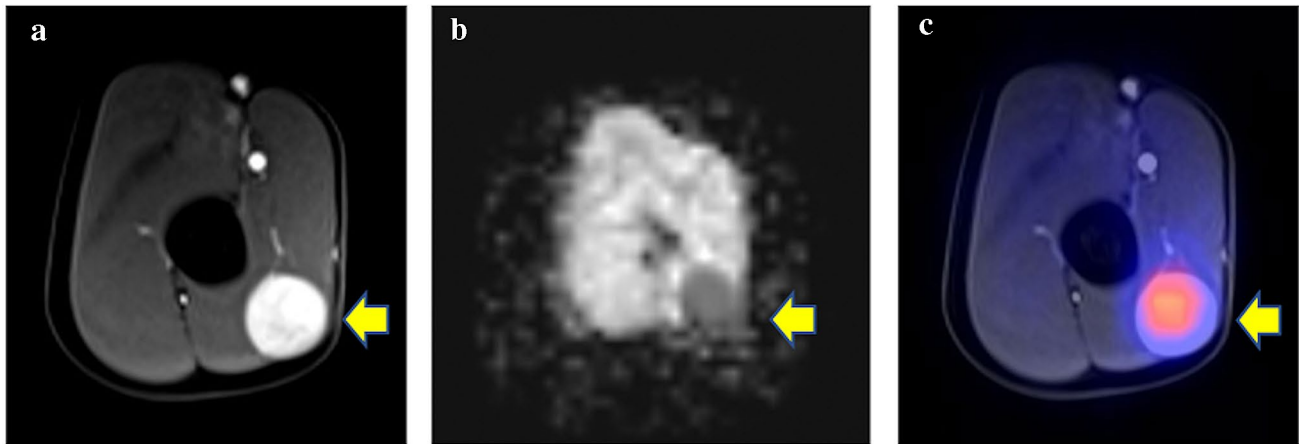
Fig. 2 Axial TIRM in (**a**) well demonstrating the rhabdomyosarcoma of the right biceps muscle affecting a 11-year-old female. The lesion demonstrated restricted diffusion (**b**) and high metabolic activity (**c**)

Since nine cases of rhabdomyosarcoma were collected, separate analyses for this group were then performed. A moderate to good significant negative correlation between ADCs' and SUVs' mean, median, and skewness ($r_{mean} = -0.541$, $r_{median} = -0.597$, $r_{skewness} = -0.568$, $p < 0.001$) occurred, whereas a poor significant positive correlation between ADCs' and SUVs' kurtosis ($r_{kurtosis} = 0.348$, $p < 0.001$) was detected.

Discussion

Our results demonstrated that there is a significant correlation between volumetric ADC and SUV values in pediatric sarcomas examined for staging. In particular, mean and median values showed a significant reciprocal correlation. This evidence is consistent with the fact that malignancies are characterized by low ADC values due to high cellularity and high SUV values caused by the high metabolic rate. Our data also in line with previous studies on adults [9]. For instance, Lahiji and colleagues showed that the extent of restricted diffusion and overlap hypermetabolism in patients with rhabdomyosarcoma have a negative predictive role [11]. Moreover, Sagiyama et al. demonstrated a negative correlation between voxel-based ADCs and SUVs values, collected by PET/MRI, which was even stronger for high grade tumors [11]. Similar results were obtained by a PET/CT and MRI study on skeletal and soft tissue tumors, using ADCmin and SUVmax values collected from a single slice ROI [12]. Such relationship emerged also for head and neck squamous carcinomas, rectal adenocarcinomas, and primary cervical cancer [8, 13–15]. On the contrary, controversial results emerged for other tumors like breast cancer or lymphomas [7, 16].

Several factors may have contributed to this heterogeneity. Firstly, some studies were performed with PET/CT and MRI [8, 13–18] without a simultaneous acquisition of data. This aspect may have influenced the measurements not only in terms of biological modifications of the lesions, but also regarding the fusion of images collected from different devices.

Secondly, most of the studies were conducted using 2D ROIs [8, 9, 19] and a single ROI approach may not properly represent the heterogeneity of the tumor. It is especially important for sarcomas because they are often characterized by necrotic and/or hemorrhagic areas, collagen fibers and mucinous fluid in addition to tumor cells [9]. Thus, our volumetric analyses provided a better insight into tumors' structure.

Among the volumetric histogram analyses that can be collected, mean, median, and standard deviation were mostly investigated in the literature. Skewness, which represents a measure of asymmetry of the probability distribution and kurtosis that reflects the tails of the distribution were assessed in a few studies [20–22]. For example, they correlated with the histological grade in endometrial cancer and were good predictors of the response to neoadjuvant chemotherapy in locally advanced rectal cancer [23, 24]. In other malignant tumors, higher skewness, and lower kurtosis were associated with higher histological grades and advanced diseases' stages [8, 20].

In our study, the significant negative correlation between the skewness of ADC and SUV values, also in the subgroup of rhabdomyosarcomas, demonstrated, as mentioned above, an overall high metabolic rate of lesions with high cellularity despite the known heterogeneous behavior of sarcomas at both, PET and at DWI.

The poor positive correlation of kurtosis does not allow us to draw precise conclusions about its role. Nevertheless,
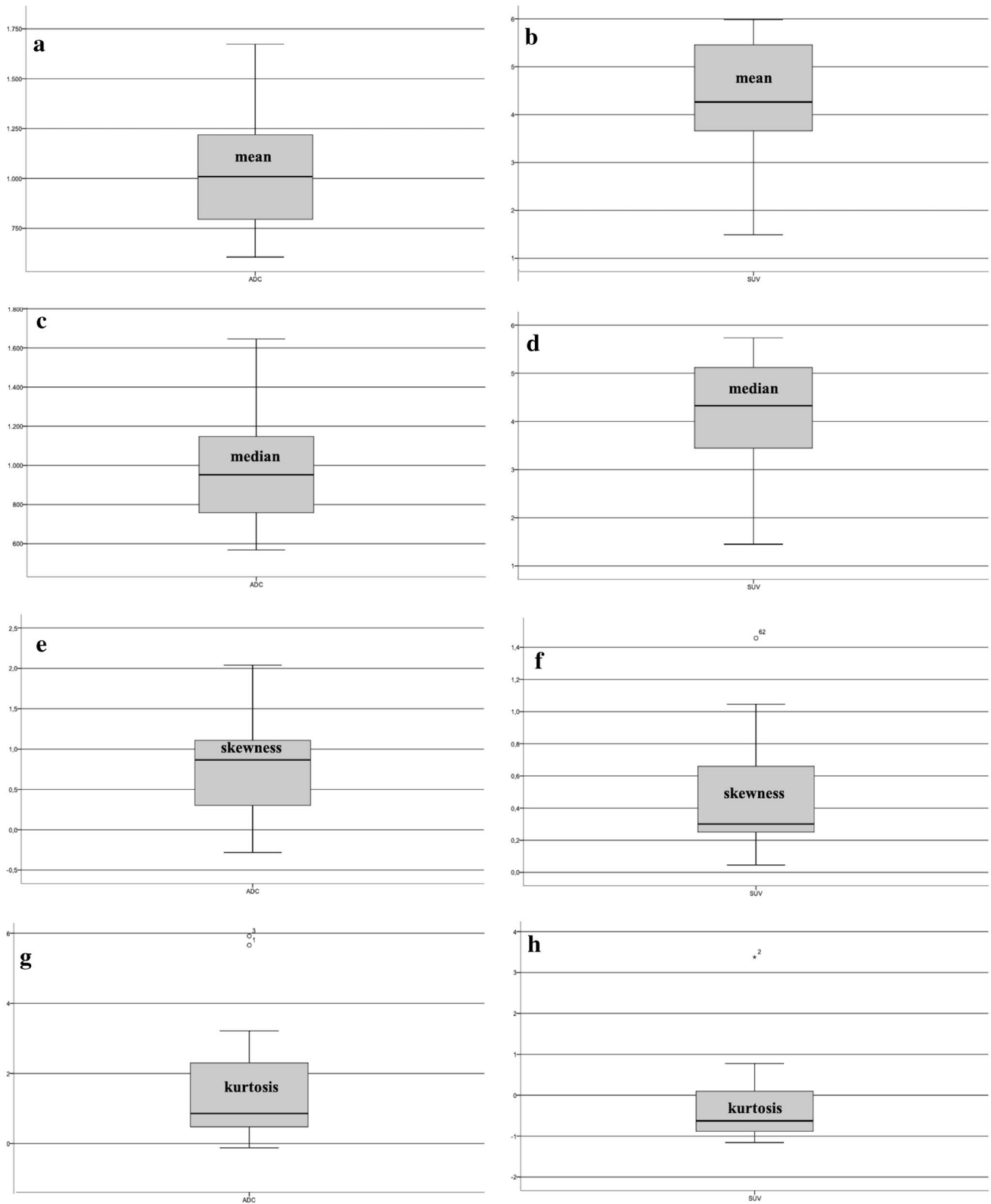
Fig. 3 Box plots representing the distribution of mean (**a**, **b**), median (**c**, **d**), skewness (**e**, **f**), and kurtosis (**g**, **h**) of the ADC and SUV values deriving from the volumetric analyses
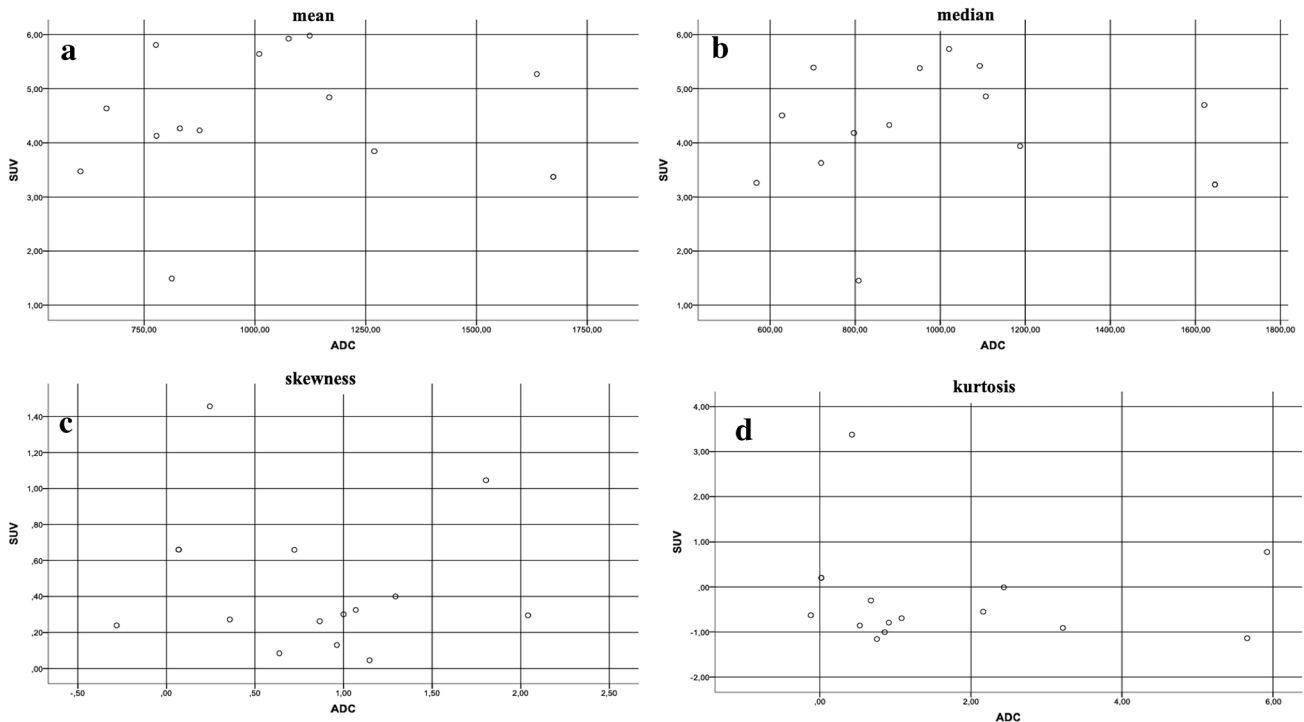
Fig. 4 Scattered plots representing the relationship between ADC's and SUV's mean (**a**), median (**b**), skewness (**c**), and kurtosis (**d**)

as previously shown, this variable could contribute to the evaluation of diseases' progression. Therefore, future studies focusing on restaging are highly encouraged [25].

Furthermore, no significant correlation was found between ADCs' and SUVs' standard deviation. This evidence might be due to the high heterogeneity of signals on the ADC map due to different components of the tumor [11]. However, a correlation between histological and radiological tumors' architecture is necessary to fully assess this evidence.

It should also be noted that neither ADCs' nor SUVs' volumetric histograms correlated with tumors' volume. This result is in agreement with the existing literature about this type of cancer. In fact, a negative correlation between tumor volume and ADC values has been reported for several tumors but sarcomas [26].

Overall, our preliminary results support the application of texture analysis in pediatric musculoskeletal imaging for staging and we call for further studies investigating its prognostic role. Moreover, we comprehensively promote the role of PET/MRI. In fact, this technique delivers a lower radiation dose, which is a key element in oncological patients undergoing long-term follow-up [27]. The use of PET/MRI may reduce the total number of examinations since it combines local and whole-body staging.

Our study is affected by several limitations. Firstly, we examined a small sample size, albeit pediatric sarcomas are rare tumors. Despite the low number of cases, we have also performed a subgroup analysis for rhabdomyosarcomas, that is the most common soft tissue sarcoma of childhood. Therefore, we can assume that our results are representative for this type of cancer.

Secondly, we did not directly correlate radiological data with histological findings, but not all patients underwent surgical resection. Future studies focused on pathological and radiological correlation may provide further insights.

Moreover, we did not perform any longitudinal analysis after treatment. Surely investigating the relationship between voxel-based SUVs and ADCs at follow-up, considering also the long-term outcome and the eventual prognostic capacity, might be of interest for the scientific community.

Our population was mainly composed of typically FDG-avid tumors, but it should not be overlooked that sarcomas are not always hypermetabolic. Thus, our results may not be considered representative for all sarcomas.

Lastly, we have used a manual segmentation which is time consuming. We call for studies, taking advantage of methods of automatic segmentation which may also promote the application of this type of analyses in the clinical practice [28].

Future perspective

The field of quantitative musculoskeletal oncological imaging is expected to further expand in the near future, taking full advantage of the most recent technical developments. For instance, the relationship between innovative/specific tracers and DWI should be investigated. In fact, several studies obtained interesting results using tracers allowing the noninvasive assessment of hypoxia such as [^{18}F]HX4 in a preclinical rhabdomyosarcoma model, ^{18}F-FMISO for brain and prostatic tumors, and $^{64/60}$Cu-ATSM, for instance, for cervical cancer and soft tissue sarcomas. Nevertheless, PET/MRI applications including complex quantitative evaluations are still missing [29–31].

Additionally, a natural progression of our work will be to evaluate the role of radiomic features collected from hybrid techniques in pediatric sarcomas. Indeed, as demonstrated for other types of tumors, this quantitative approach may expand our knowledge about tumors characteristics [32, 33].

Last, the application of PET/MRI is also expected to explore the benefit of additional techniques like tumors perfusion, MR spectroscopy, intravoxel incoherent motion in association with the simultaneous assessment of tumors' metabolic activity [34, 35].

In conclusion, according to our preliminary PET/MRI study, volumetric simultaneously collected SUVs and ADCs are dependent biomarkers in FDG-avid sarcomas. Further studies including the response to treatment are necessary to fully assess the clinical impact of this evidence.

Declarations

Conflict of interest None of the authors has any conflict of interest to declare.

Informed consent All patients' parents gave written informed consent before imaging.

Ethical approval This retrospective study was approved by the Institutional Review Board. All procedures in studies involving human participants were in accordance with the ethical standards of the institutional and/or national research committee and with the 1964 Declaration of Helsinki and its later amendments or comparable ethical standards.

References

1. Williams RF, Fernandez-Pineda I, Gosain A (2016) Pediatric sarcomas. Surg Clin North Am 96:1107–1125

2. Egas-Bejar D, Huh WW (2016) Rhabdomyosarcoma in adolescent and young adult patients: current perspectives. Adolesc Health Med Ther 5:115–125

3. Qureshi SS, Bhagat M (2015) Non-rhabdomyosarcoma soft-tissue sarcomas in children: Contemporary appraisal and experience from a single centre. J Indian Assoc Pediatr Surg 20:165–169

4. Torigian DA, Zaidi H, Kwee TC, Saboury B, Udupa JK, Cho ZH, Alavi A (2013) PET/MR imaging: technical aspects and potential clinical applications. Radiology 267:26–44

5. Luna A, Pahwa S, Bonini C, Alcalá-Mata L, Wright KL, Gulani V (2016) Multiparametric MR imaging in abdominal malignancies. Magn Reson Imaging Clin N Am 24:157–186

6. Giraudo C, Raderer M, Karanikas G et al (2016) 18F-fluorodeoxyglucose positron emission tomography/magnetic resonance in lymphoma: comparison with 18F-fluorodeoxyglucose positron emission tomography/computed tomography and with the addition of magnetic resonance diffusion-weighted imaging. Invest Radiol 51:163–169

7. Giraudo C, Karanikas G, Weber M et al (2018) Correlation between glycolytic activity on [18F]-FDG-PET and cell density on diffusion-weighted MRI in lymphoma at staging. J Magn Reson Imaging 47:1217–1226

8. Deng S, Wu Z, Wu Y et al (2017) Meta-analysis of the correlation between apparent diffusion coefficient and standardized uptake value in malignant disease. Contrast Media Mol Imaging 2017:4729547

9. Sagiyama K, Watanabe Y, Kamei R et al (2017) Multiparametric voxel-based analyses of standardized uptake values and apparent diffusion coefficients of soft-tissue tumours with a positron emission tomography/magnetic resonance system: Preliminary results. Eur Radiol 27:5024–5033

10. Rasmussen JH, Nørgaard M, Hansen AE et al (2017) Feasibility of multiparametric imaging with PET/MR in head and neck squamous cell carcinoma. J Nucl Med 58:69–74

11. Lahji AP, Jackson T, Nejadnik H et al (2019) Association of Tumor [18F]FDG Activity and Diffusion Restriction with Clinical Outcomes of Rhabdomyosarcomas. Mol Imaging Biol 21:591Y598

12. Lee SY, Jee WH, Yoo IR et al (2019) Comparison of 3T diffusion-weighted MRI and 18F-FDG PET/CT in musculoskeletal tumours: quantitative analysis of apparent diffusion coefficients and standardized uptake values. Br J Radiol 92:20181051

13. Nakajo M, Nakajo M, Kajiya Y et al (2012) FDG PET/CT and diffusion-weighted imaging of head and neck squamous cell carcinoma: comparison of prognostic significance between primary tumor standardized uptake value and apparent diffusion coefficient. Clin Nucl Med 37:475–480

14. Er HÇ, Erden A, Küçük NÖ, Geçim E (2014) Correlation of minimum apparent diffusion coefficient with maximum standardized uptake on fluorodeoxyglucose PET-CT in patients with rectal adenocarcinoma. Diagn Interv Radiol 20:105–109

15. Grueneisen J, Beiderwellen K, Heusch P et al (2014) Correlation of standardized uptake value and apparent diffusion coefficient in integrated whole-body PET/MRI of primary and recurrent cervical cancer. PLoS ONE 9:e96751

16. Kitajima K, Yamano T, Fukushima K et al (2016) Correlation of the SUVmax of FDG-PET and ADC values of diffusion-weighted MR imaging with pathologic prognostic factors in breast carcinoma. Eur J Radiol 85:943–949

17. Rakheja R, Chandarana H, DeMello L et al (2013) Correlation between standardized uptake value and apparent diffusion coefficient of neoplastic lesions evaluated with whole-body simultaneous hybrid PET/MRI. AJR Am J Roentgenol 201:1115–1119

18. Baba S, Isoda T, Maruoka Y et al (2014) Diagnostic and prognostic value of pretreatment SUV in 18F-FDG/PET in breast cancer: comparison with apparent diffusion coefficient from diffusion-weighted MR imaging. J Nucl Med 55:736–742

19. Schmidt H, Brendle C, Schraml C et al (2013) Correlation of simultaneously acquired diffusion-weighted imaging and 2-deoxy-[18F] fluoro-2-D-glucose positron emission tomography of pulmonary lesions in a dedicated whole-body magnetic resonance/positron emission tomography system. Invest Radiol 48:247–255

20. Baek HJ, Kim HS, Kim N, Choi YJ, Kim YJ (2012) Percent change of perfusion skewness and kurtosis: a potential imaging biomarker for early treatment response in patients with newly diagnosed glioblastomas. Radiology 264:834–843

21. Downey K, Riches SF, Morgan VA et al (2013) Relationship between imaging biomarkers of stage I cervical cancer and poor-prognosis histologic features: quantitative histogram analysis of diffusion-weighted MR images. AJR Am J Roentgenol 200:314–320

22. King AD, Chow KK, Yu KH et al (2013) Head and neck squamous cell carcinoma: diagnostic performance of diffusion-weighted MR imaging for the prediction of treatment response. Radiology 266:531–538

23. Woo S, Cho JY, Kim SY, Kim SH (2014) Histogram analysis of apparent diffusion coefficient map of diffusion-weighted MRI in endometrial cancer: a preliminary correlation study with histological grade. Acta Radiol 55:1270–1277

24. Enkhbaatar NE, Inoue S, Yamamuro H et al (2018) MR imaging with apparent diffusion coefficient histogram analysis evaluation of locally advanced rectal cancer after chemotherapy and radiation therapy. Radiology 288:129–137

25. Gennaro N, Marrari A, Renne SL et al (2020) Multimodality imaging of adult rhabdomyosarcoma: the added value of hybrid imaging. Br J Radiol 93:20200250

26. Husby JA, Salvesen ØO, Magnussen IJ et al (2015) Tumour apparent diffusion coefficient is associated with depth of myometrial invasion and is negatively correlated to tumour volume in endometrial carcinomas. Clin Radiol 70:487–494

27. States LJ, Reid JR (2020) Whole-body PET/MRI applications in pediatric oncology. AJR 215:713–725

28. Garrison KA, Rogalsky C, Sheng T et al (2015) Functional MRI preprocessing in lesioned brains: manual versus automated region of interest analysis. Front Neurol 6:196

29. Imam SK (2010) Review of positron emission tomography tracers for imaging of tumor hypoxia. Cancer Biother Radiopharm 25:365–374

30. Peeters SGJA, Zegers CML, Lieuwes NG et al (2014) A comparative study of the hypoxia PET tracers [18F]HX4, [18F]FAZA, and [18F]FMISO in a preclinical tumor model. Int J Radiat Oncol Biol Phys 91:351–359

31. Dubois L, Landuyt W, Haustermans K et al (2004) Evaluation of hypoxia in an experimental rat tumour model by [(18)f]fluoromisonidazole pet and immunohistochemistry. Br J Cancer 91:1947–1954

32. Mayerhoefer M, Riedl CC, Kumar A et al (2019) Radiomic features of glucose metabolism enable prediction of outcome in mantle cell lymphoma. Eur J Nucl Med Mol Imaging 46:2760–2769

33. Maldonado F, Varghese C, Rajagopalan S et al (2020) Validation of the BRODERS classifier (Benign versus aggressive nODule evaluation using radiomic stratification), a novel high-resolution computed tomography-based radiomic classifier for indeterminate pulmonary nodules. Eur Respir J 10:2002485

34. Wu G, Liu X, Xiong Y et al (2018) Intravoxel incoherent motion and diffusion kurtosis imaging for discriminating soft tissue sarcoma from vascular anomalies. Medicine 97(50):e13641

35. Vilanova JC, Baleato-Gonzalez S, Romero MJ, Carrascoso-Arranz J, Luna A (2016) Assessment of musculoskeletal malignancies with functional MR imaging. Magn Reson Imaging Clin N Am 24:239–259